Diffusion tensor imaging of lumbar nerve roots: Comparison between fast readout-segmented and selective-excitation acquisitions

Manoliu, Andrei ; Ho, Michael ; Nanz, Daniel ; Piccirelli, Marco ; Dappa, Evelyn ; Klarhöfer, Markus ; Del Grande, Filippo ; Kuhn, Felix Pierre

Abstract: OBJECTIVES: The aim of this study was to compare the quality of recently emerged advanced diffusion tensor imaging (DTI) techniques with conventional single-shot echo-planar imaging (EPI) in a functional assessment of lumbar nerve roots. MATERIALS AND METHODS: The institutional review board approved the study including 12 healthy volunteers. Diffusion tensor imaging was performed at 3 T (MAGNETOM Skyra; Siemens Healthcare) with b-values of 0 and 700 s/mm and an isotropic spatial resolution for subsequent multiplanar reformatting. The nerve roots L2 to S1 were imaged in coronal orientation with readout-segmented EPI (rs-DTI) and selective-excitation EPI (sTX-DTI) with an acquisition time of 5 minutes each, and in axial orientation with single-shot EPI (ss-DTI) with an acquisition time of 12 minutes (scan parameters as in recent literature). Two independent readers qualitatively and quantitatively assessed image quality. RESULTS: The interobserver reliability ranged from "substantial" to "almost perfect" for all examined parameter and all 3 sequences (= 0.70-0.94). Overall image quality was rated higher, and artifact levels were scored lower for rs-DTI and sTX-DTI than for ss-DTI (P = 0.007-0.027), while fractional anisotropy and signal-to-noise ratio values were similar for all sequences (P 0.306 and P 0.100, respectively). Contrast-to-noise ratios were significantly higher for rs-DTI and ss-DTI than for sTX-DTI (P = 0.004-0.013). CONCLUSIONS: Despite shorter acquisition times, rs-DTI and sTX-DTI produced images of higher quality with smaller geometrical distortions than the current standard of reference, ss-DTI. Thus, DTI acquisitions in the coronal plane, requiring fewer slices for full coverage of exiting nerve roots, may allow for functional neurography in scan times suitable for routine clinical practice.

DOI: https://doi.org/10.1097/RLI.0000000000000260

Diffusion Tensor Imaging of Lumbar Nerve Roots
Comparison Between Fast Readout-Segmented and Selective-Excitation Acquisitions

Andrei Manoliu, MD, PhD, Michael Ho, MD,* Daniel Nanz, PhD,* Marco Piccirelli, PhD,† Evelyn Dappa, MD,* Markus Klarhöfer, PhD,‡ Filippo Del Grande, MD, MBA,§ and Felix Pierre Kuhn, MD, MAS**

Objectives: The aim of this study was to compare the quality of recently emerged advanced diffusion tensor imaging (DTI) techniques with conventional single-shot echo-planar imaging (EPI) in a functional assessment of lumbar nerve roots.
Materials and Methods: The institutional review board approved the study including 12 healthy volunteers. Diffusion tensor imaging was performed at 3 T (MAGNETOM Skyra; Siemens Healthcare) with *b*-values of 0 and 700 s/mm^2 and an isotropic spatial resolution for subsequent multiplanar reformatting. The nerve roots L2 to S1 were imaged in coronal orientation with readout-segmented EPI (rs-DTI) and selective-excitation EPI (sTX-DTI) with an acquisition time of 5 minutes each, and in axial orientation with single-shot EPI (ss-DTI) with an acquisition time of 12 minutes (scan parameters as in recent literature). Two independent readers qualitatively and quantitatively assessed image quality.
Results: The interobserver reliability ranged from "substantial" to "almost perfect" for all examined parameter and all 3 sequences ($\kappa = 0.70$–0.94). Overall image quality was rated higher, and artifact levels were scored lower for rs-DTI and sTX-DTI than for ss-DTI ($P = 0.007$–0.027), while fractional anisotropy and signal-to-noise ratio values were similar for all sequences ($P \geq 0.306$ and $P \geq 0.100$, respectively). Contrast-to-noise ratios were significantly higher for rs-DTI and ss-DTI than for sTX-DTI ($P = 0.004$–0.013).
Conclusions: Despite shorter acquisition times, rs-DTI and sTX-DTI produced images of higher quality with smaller geometrical distortions than the current standard of reference, ss-DTI. Thus, DTI acquisitions in the coronal plane, requiring fewer slices for full coverage of exiting nerve roots, may allow for functional neurography in scan times suitable for routine clinical practice.

Key Words: MR neurography, DTI techniques, DTI peripheral nerves, lumbar spine, lumbar nerve roots

(*Invest Radiol* 2016;00: 00–00)

The diagnosis of nerve root entrapment in patients with irradiating chronic low back pain is challenging, and morphological state-of-the art magnetic resonance (MR) imaging often fails to reliably identify a potential conflict.[1,2] Recent studies have shown that diffusion tensor imaging (DTI) of the lumbar nerve roots lowers the number of false-positive and false-negative findings and thus increases the concordance between imaging and clinical findings.[3–5] Diffusion tensor imaging adds important information on the integrity of neuronal fibers on a molecular level[6–13] not available from conventional MR imaging. However, rather long acquisition times prevented this functional MR neurography technique from being implemented in clinical routine.

Lowering the number of acquired slices can efficiently shorten scan time. A full coverage of the symmetrically exiting nerve roots in the lumbar spine, L2 to S1, requires fewer coronal than axial slices. However, standard acquisitions in coronal orientation need to cover the full left-to-right body extension, potentially including the arms, to avoid aliasing. The large field of view (FOV) in combination with small isotropic voxel size results in very long echo trains when standard single-shot echo-planar imaging is used for DTI data acquisition (ss-DTI). Concomitantly, strong susceptibility-related artifacts, such as geometric distortions and signal loss due to spin dephasing result. Consequently, all recently published DTI studies of lumbar nerve roots sampled DTI data in the axial plane.[3,4,14–16]

An alternative technique is to divide the k-space trajectory into multiple segments along the readout direction (rs-DTI).[17–19] This requires multiple excitations followed by shorter echo trains, each of which only samples part of the raw data for a single image. The segmentation results in shorter minimum echo times, increasing the signal-to-noise ratio (SNR), and significantly reduces the severity of susceptibility-related artifacts. A potential drawback inherent to multishot approaches is artifacts caused by intershot displacement of anatomy.

Another promising image acquisition scheme exploits dynamic parallel transmit selective-excitation technology (sTX-DTI).[20–24] Multichannel parallel spin excitation can excite spins in arbitrarily shaped volumes and parts of image slices instead of complete image slices, while still keeping the excitation pulses and echo times reasonably short. This allows a reduction of the FOV along the phase-encoding direction without causing aliasing. Furthermore, it can result in less severe geometric distortion and blurring artifacts, due to shorter echo trains, less motion and flow artifacts, as tissue outside the reduced FOV is not excited, and shorter scan times as fewer phase-encoding lines are required to obtain the same spatial resolution.

The purpose of this study was to compare the image quality of these advanced DTI techniques applied in coronal section orientations with conventional axial single-shot echo-planar imaging DTI in the functional assessment of lumbar nerve roots.

MATERIALS AND METHODS

The local ethics board approved this prospective study, and all volunteers provided written informed consent. Twelve volunteers were examined (6 women: mean [SD] age, 25.50 [3.30] years [age range, 19–29 years]; 6 men: age mean [SD], 31.16 [4.70] years [age range, 26–40 years]). Inclusion criteria were age older than 18 years and good physical health. Exclusion criteria were contraindication to MR, acute or chronic low back pain, or experience of sciatica.

Image Acquisition

Morphological and diffusion tensor images of lumbar nerve roots were acquired on a 3 T MR system (MAGNETOM Skyra; Siemens Healthcare, Erlangen, Germany) between January and May 2015. Two

Received for publication November 27, 2015; and accepted for publication, after revision, December 28, 2015.
From the *Institute of Diagnostic and Interventional Radiology, and †Department of Neuroradiology, University Hospital Zurich, University of Zurich; ‡Siemens Healthcare AG, Zurich; and §Institute of Diagnostic Radiology, Regional Hospital Lugano, Lugano, Switzerland.
Conflicts of interest and sources of funding: This research was partially funded by the Young Researchers Grant awarded by the European Society of Musculoskeletal Radiology (A.M.) and the Olga Mayenfisch Stiftung. No industry support was received for this study. Markus Klarhöfer is an employee of Siemens Healthcare AG, Zurich, Switzerland. For the remaining authors, none were declared.
Andrei Manoliu and Michael Ho contributed equally to this work.
This was a prospective institutional review board–approved magnetic resonance imaging study. It included imaging of asymptomatic healthy volunteers. All volunteers gave written informed consent.
Correspondence to: Felix Pierre Kuhn, MD, MAS, Institute of Diagnostic and Interventional Radiology, University Hospital Zurich, Raemistrasse 100, CH-8091 Zurich, Switzerland. E-mail: Felix.Kuhn@usz.ch.

ISSN: 0020-9996/16/0000–0000
DOI: 10.1097/RLI.0000000000000260

TABLE 1. Sequence Parameters

	ss-DTI	rs-DTI	sTX-DTI
b-value 1/2, s/mm^2	0/700	0/700	0/700
TR, ms	5700	4650	4700
TE, ms	65	63	78
Matrix	80 × 80	96 × 96	96 × 37
FOV, mm^2	166 × 166	200 × 200	200 × 75
In-plane resolution, mm^2	2.1 × 2.1	2.1 × 2.1	2.1 × 2.1
No. slices	44	29	29
Stacks	2	1	1
Slice thickness, mm	2.1	2.1	2.1
Acceleration factor (iPAT)	2	2	2
Pixel bandwidth, Hz/Px	1894	930	1860
Acquisition time, min:s	12:24	5:04	5:07

ss-DTI indicates single-shot echo-planar diffusion tensor imaging; rs-DTI, readout-segmented echo-planar diffusion tensor imaging; sTX-DTI, selective-excitation accelerated echo-planar diffusion tensor imaging with reduced field of view; TR, repetition time; TE, echo time; FOV, field of view; iPAT, integrated parallel acquisition techniques.

channels allowed for independent parallel transmission (TimTX TrueShape; Siemens Healthcare) and an 18-channel phased array spine coil received the signal.

Three DTI data sets were acquired: (1) ss-DTI images in the axial plane with scan parameters in accordance with recent literature[3,14,15] as standard of reference, (2) rs-DTI images in the coronal plane with navigator echo correction (RESOLVE; Siemens Healthcare), and (3) sTX-DTI images in the coronal plane with reduced volume excitation (ZOOMit; Siemens Healthcare). All DTI sequences acquired voxels with isotropic diameters of 2.1 mm for subsequent multiplanar reformatting. *b*-Values were set to 0 and 700 s/mm^2.[25] Integrated parallel acquisition techniques were applied to all DTI sequences with a GRAPPA acceleration factor of 2. Total acquisition time corresponded to 12 minutes and 24 seconds for ss-DTI, 5 minutes and 4 seconds for rs-DTI, and 5 minutes and 7 seconds for sTX-DTI. Pulse sequence-specific DTI parameters are summarized in Table 1.

T2-weighted (T2w) turbo-spin echo images with spectral attenuated inversion recovery (SPAIR) fat suppression were acquired in coronal orientation for anatomical correlation with the following sequence parameters: repetition time = 4000 milliseconds; echo time = 95 milliseconds; voxel size = 0.3 × 0.3 × 2.1 mm^3; number of slices = 29; FOV = 260 × 260 mm; receive bandwidth = 250 Hz/Px.

Image Analysis

Images were postprocessed on the syngo.via platform (Version VB10A; Siemens Healthcare, Erlangen, Germany). Two independent readers made a qualitative and quantitative image assessment (reader 1, A.M., research fellow in musculoskeletal radiology with a PhD in neuroimaging; reader 2, F.P.K., clinical fellow in musculoskeletal radiology with 2 years' training in neuroradiology). Diffusion tensor imaging trace images were assessed in overlay mode with T2w images to grade potential geometrical distortions due to susceptibility variations and consequent spatial misregistration (semiquantitative 5-point Likert scale: 1, none; 2, low; 3, moderate; 4, high; 5, very high), to rate overall image quality (1, excellent; 2, good; 3, moderate; 4, poor; 5, nondiagnostic) and to determine the contrast between the nerve root intensities (I) and the surrounding muscles ($C = \frac{I(nerve)-I(muscle)}{I(nerve)+I(muscle)}$). Contrast was measured by placing an elliptic region of interest (ROI) into the nerve root ganglion

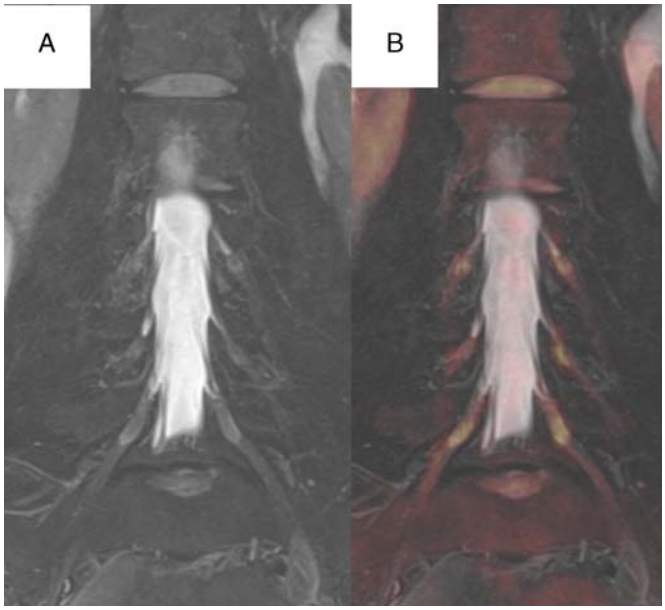

FIGURE 1. Anatomical correlation of diffusion tensor imaging of the spine for a 29-year-old female volunteer. A, Panel shows a T2w turbo-spin echo image with spectral attenuated inversion recovery fat suppression of the lumbar spine. B, Panel demonstrates the projection of a readout-segmented diffusion tensor imaging trace map (red) on the corresponding T2w image (gray scale) in the same volunteer. Figure 1 can be viewed online in color at www.investigativeradiology.com.

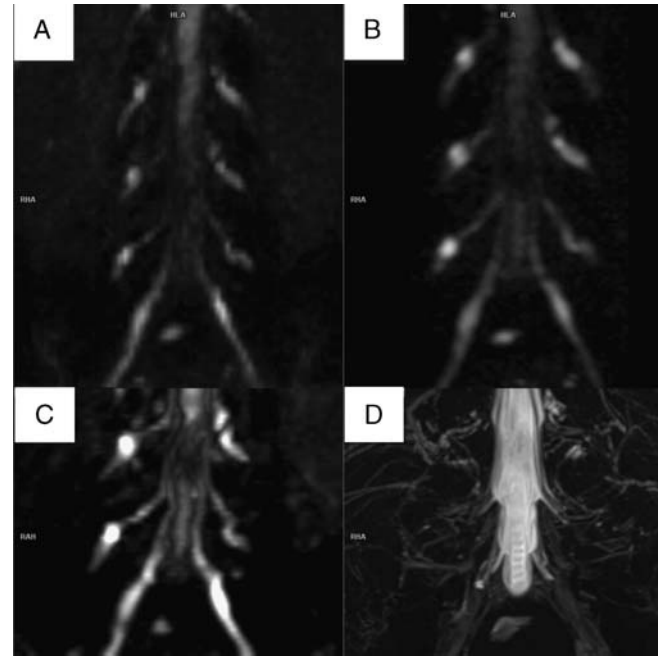

FIGURE 2. Diffusion tensor imaging of the lumbar spine for a 27-year-old male healthy volunteer using different diffusion sequences. A, Coronal readout-segmented diffusion tensor imaging (rs-DTI, *b*-value = 700). B, Coronal selective-excitation accelerated diffusion tensor imaging with reduced FOV (sTX-DTI, *b*-value = 700). C, Reformatted axial single-shot echo-planar diffusion tensor imaging (ss-DTI, *b*-value = 700). A–C, Maximum intensity projections are shown (slab thickness, 10.0 mm). Overall image quality was rated "excellent" by both readers for rs-DTI (A) and sTX-DTI (B) and "moderate" for ss-DTI (C). D, The panel shows a T2w turbo-spin echo image with spectral attenuated inversion recovery fat suppression for anatomical correlation.

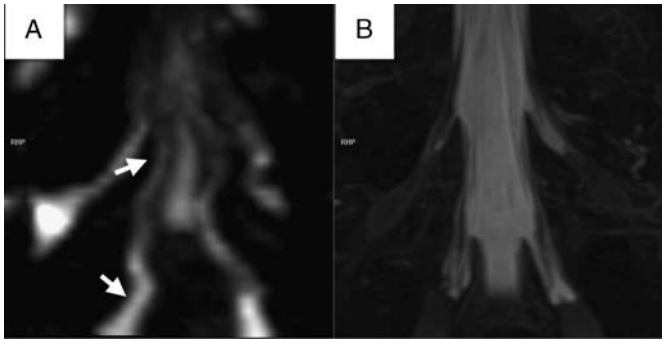

FIGURE 3. Distortion artifacts observed with single-shot echo-planar diffusion tensor imaging for a 34-year-old male healthy volunteer. A, The panel shows a maximum intensity projection for single-shot diffusion tensor imaging. B, The panel corresponds to T2-weighted turbo-spin echo image with spectral attenuated inversion recovery for anatomical correlation. In this case, geometrical distortion artifacts were graded as "moderate" by reader 1 and "high" by reader 2.

L4 and in the adjacent psoas muscle on both sides. The ROI size was adjusted to the nerve root size to minimize partial volume effects. For contrast-to-noise ratio (CNR) analyses, the contrast was divided by the estimated noise σ (see Signal-to-Noise Ratio section). For SNR analysis, each reader placed an ROI for each subject on the $b = 0$ s/mm^2 images into an area of homogeneous signal within the intervertebral disc between the fourth and fifth lumbar vertebra. Subsequently, the mean signal intensity and the corresponding standard deviation were extracted. The SNR was estimated as the ratio of mean signal intensity of the ROI and its standard deviation. Nerve root integrity was quantitatively assessed by measuring intraforaminal fractional anisotropy (FA) values at the location of the nerve root ganglion. The quantitative results were compared with those obtained with the standard of reference acquisition and to reference values in recent literature.[3,14,15]

Statistical Analysis

All statistical tests were performed using the SPSS statistics software (SPSS Version 21; IBM Corp). Interreader agreement was assessed by calculating intraclass correlation coefficients (ICCs) for CNR and SNR and by calculating Cohen κ for the overall image quality and artifacts scores. Cohen κ values were interpreted according to Landis and Koch,[26] and ICC values according to Kundel and Polanski.[27] Normal distribution of CNR and SNR was evaluated using the Shapiro-Wilk test (significance level $\alpha = 0.05$). Paired sample t tests were used to evaluate for statistically significant between-group differences regarding CNR, SNR, and FA (significance level $\alpha = 0.05$). To assess potential intergroup differences with respect to the overall image quality and artifacts, Wilcoxon signed rank tests were performed (significance level $\alpha = 0.05$). All statistical tests were Bonferroni corrected for multiple comparisons, where applicable.

RESULTS

All images were successfully acquired in all healthy volunteers without exceeding the individual limits of the specific absorption rate (Fig. 1). The interobserver reliability ranged from "substantial" to "almost perfect" for artifact severity (sTX-DTI, κ = 0.851; rs-DTI, κ = 0.825; ss-DTI, κ = 0.783) as well as for the overall image quality (sTX-DTI, κ = 0.851; rs-DTI, κ = 0.697; ss-DTI, κ = 0.787). For both readers, overall image quality for rs-DTI was significantly higher (R1, $P = 0.013$; R2, $P = 0.007$; Fig. 2) and the artifact scores lower (R1, $P = 0.007$; R2, $P = 0.017$; Fig. 3) than for ss-DTI (Table 2). Equally, overall image quality (R1, $P = 0.023$; R2, $P = 0.013$) and artifact scores for sTX-DTI were significantly lower (R1, $P = 0.027$; R2, $P = 0.020$; see also Table 2) than for ss-DTI for both readers. There was no statistically significant difference with respect to artifacts or overall image quality between rs-DTI and sTX-DTI for both readers.

Contrast-to-Noise Ratio

Interobserver reliability was "almost perfect" for sTX-DTI (ICC = 0.911), rs-DTI (ICC = 0.940), and ss-DTI (ICC = 0.897). The CNR values were normally distributed for both readers and all sequences (R1, $P \geq 0.081$; R2, $P \geq 0.090$). Contrast-to-noise ratio values were significantly higher for rs-DTI than for sTX-DTI for both readers (R1, $P = 0.013$; R2, $P = 0.004$). For 1 reader, they were also significantly higher for ss-DTI than for sTX-DTI (R2, $P = 0.0005$), even after correction for multiple comparisons (n = 3). For both readers, there were no statistically significant difference in CNR between rs-DTI and ss-DTI (see Table 3 for a detailed presentation of the CNR characteristics for both readers and all sequences as well as corresponding between group differences).

Signal-to-Noise Ratio

The interobserver reliability was "almost perfect" for sTX-DTI (ICC = 0.893), rs-DTI (ICC = 0.822), and ss-DTI (ICC = 0.827). Signal-to-noise ratio values were normally distributed for both readers and all sequences (R1, $P \geq 0.120$; R2, $P \geq 0.142$). In general, SNR

TABLE 2. Qualitative Analysis

	ss-DTI		rs-DTI		sTX-DTI		ss-DTI vs rs-DTI	ss-DTI vs sTX-DTI	rs-DTI vs sTX-DTI
	Mean	SD	Mean	SD	Mean	SD	*P*	*P*	*P*
Reader 1									
Artifacts	3.70	0.48	2.10	0.74	2.60	1.17	0.007*	0.027*	0.096
Image quality	3.50	0.85	2.10	0.57	2.30	1.06	0.013*	0.023*	0.414
Reader 2									
Artifacts	3.60	0.52	2.30	0.95	2.50	1.08	0.017*	0.020*	0.317
Image quality	3.60	0.70	2.10	0.57	2.20	1.03	0.007*	0.013*	0.655

Grading of artifacts and overall image quality is given for each sequence and reader as mean (SD) on a 5-point Likert scale (artifacts: 1, none; 2, low; 3, moderate; 4, high; 5, very high; overall image quality: 1, excellent; 2, good; 3, moderate; 4, poor; 5, nondiagnostic). Wilcoxon signed rank tests were performed to assess potential between group differences. Corresponding *P* values are given.

*Statistical significance ($P < 0.05$).

ss-DTI indicates single-shot echo-planar diffusion tensor imaging; rs-DTI, readout-segmented echo-planar diffusion tensor imaging; sTX-DTI, selective-excitation accelerated echo-planar diffusion tensor imaging with reduced field of view.

TABLE 3. Quantitative CNR and SNR Analysis

	ss-DTI		rs-DTI		sTX-DTI		ss-DTI vs rs-DTI	ss-DTI vs sTX-DTI	rs-DTI vs sTX-DTI
	Mean	SD	Mean	SD	Mean	SD	*P*	*P*	*P*
Reader 1									
CNR	0.658	0.150	0.738	0.136	0.562	0.178	0.251	0.088	0.013
SNR	10.211	3.042	11.907	4.201	13.055	5.547	0.295	0.221	0.682
Reader 2									
CNR	0.675	0.148	0.730	0.125	0.529	0.142	0.385	0.001	0.005
SNR	9.594	3.098	12.636	4.166	13.175	5.429	0.097	0.140	0.833

For each sequence and reader, CNR and SNR are given as mean (SD). Paired sample *t* tests were performed to assess potential between group differences. Corresponding *P* values are given.

CNR indicates contrast-to-noise ratio; SNR, signal-to-noise ratio; ss-DTI, single-shot echo-planar diffusion tensor imaging; rs-DTI, readout-segmented echo-planar diffusion tensor imaging; sTX-DTI, selective-excitation accelerated echo-planar diffusion tensor imaging with reduced field of view.

was similar for all sequences (R1, $P \geq 0.220$; R2, $P \geq 0.100$; see Table 3).

Fractional Anisotropy

Fractional anisotropy values were similar for both readers (paired sample *t* test; ss-DTI, $P = 0.393$; rs-DTI, $P = 0.306$; sTX-DTI, $P = 0.962$), and all sequences with no statistically significant differences for both readers between ss-DTI and rs-DTI (R1, $P = 0.208$; R2, $P = 0.341$), between ss-DTI and sTX-DTI (R1, $P = 0.546$; R2, $P = 0.606$), or between rs-DTI and sTX-DTI (R1, $P = 0.292$; R2, $P = 0.568$; see Table 4). It is to note that the right L4 nerve root showed a trend toward higher FA for ss-DTI compared with sTX-DTI for reader 1 and that the right L3 and S1 nerve root showed a trend toward higher FA for ss-DTI compared with rs-DTI for reader 2. However, these results were not significant after correction for multiple comparisons (Bonferroni correction for multiple comparisons, n = 9 according to the number of performed tests, see also Table 4 for extensive presentation of between-group analysis for every nerve root, respectively).

DISCUSSION

Our results support the hypothesis that advanced DTI techniques with innovative excitation and sampling methods permit functional MR

TABLE 4. Quantitative Diffusion Analysis

	ss-DTI		rs-DTI		sTX-DTI		ss-DTI vs rs-DTI		ss-DTI vs sTX-DTI		rs-DTI vs sTX-DTI	
	Mean	SD	Mean	SD	Mean	SD	*P* (Uncorrected)	*P* (Corrected)	*P* (Uncorrected)	*P* (Corrected)	*P* (Uncorrected)	*P* (Corrected)
Reader 1												
L3 right	0.298	0.021	0.324	0.029	0.318	0.023	0.116	1.000	0.067	0.603	0.563	1.000
L4 right	0.328	0.020	0.308	0.023	0.302	0.019	0.048*	0.432	0.035*	0.315	0.54	1.000
L5 right	0.314	0.019	0.327	0.025	0.368	0.184	0.121	1.000	0.39	1.000	0.486	1.000
S1 right	0.300	0.029	0.327	0.048	0.316	0.031	0.170	1.000	0.275	1.000	0.534	1.000
L3 left	0.317	0.032	0.334	0.032	0.317	0.021	0.111	0.999	0.988	1.000	0.141	1.000
L4 left	0.306	0.029	0.310	0.032	0.319	0.027	0.560	1.000	0.307	1.000	0.582	1.000
L5 left	0.302	0.098	0.313	0.022	0.318	0.021	0.739	1.000	0.641	1.000	0.648	1.000
S1 left	0.321	0.039	0.320	0.030	0.275	0.091	0.980	1.000	0.128	1.000	0.171	1.000
Total	0.311	0.043	0.321	0.319	0.317	0.076	0.208	1.000	0.546	1.000	0.292	1.000
Reader 2												
L3 right	0.303	0.019	0.328	0.035	0.317	0.041	0.036*	0.324	0.318	1.000	0.467	1.000
L4 right	0.322	0.031	0.318	0.025	0.307	0.022	0.767	1.000	0.158	1.000	0.244	1.000
L5 right	0.309	0.021	0.304	0.025	0.314	0.033	0.580	1.000	0.633	1.000	0.406	1.000
S1 right	0.313	0.024	0.342	0.040	0.321	0.034	0.012*	0.108	0.509	1.000	0.067	0.603
L3 left	0.309	0.026	0.315	0.038	0.316	0.020	0.763	1.000	0.548	1.000	0.902	1.000
L4 left	0.328	0.021	0.328	0.024	0.318	0.025	0.999	1.000	0.327	1.000	0.414	1.000
L5 left	0.319	0.030	0.309	0.033	0.322	0.022	0.396	1.000	0.796	1.000	0.249	1.000
S1 left	0.317	0.032	0.313	0.053	0.321	0.042	0.849	1.000	0.743	1.000	0.643	1.000
Total	0.315	0.026	0.320	0.036	0.317	0.030	0.341	1.000	0.606	1.000	0.568	1.000

For each sequence and reader, FA values are given as mean (SD). Paired sample *t* tests were performed to assess potential between group differences. Corresponding *P* values are given uncorrected as well as Bonferroni corrected for multiple comparisons (n = 9). After Bonferroni correction for multiple comparisons, statistical analysis yielded no significant results.

*Uncorrected $P < 0.05$.

ss-DTI indicates single-shot echo-planar diffusion tensor imaging; rs-DTI, readout-segmented echo-planar diffusion tensor imaging; sTX-DTI, selective-excitation accelerated echo-planar diffusion tensor imaging with reduced field of view.

neurography of lumbar nerve roots in a reasonable scan time for routine clinical practice.

Both techniques, rs-DTI and sTX-DTI, robustly imaged nerve roots in coronal acquisitions with slightly better overall image quality and less-severe geometrical distortion artifacts than in axially acquired reference ss-DTI images. However, primarily due to the lower number of slices, the coronal acquisitions shortened the MR measurement time by a factor of 2.4, while the risk of unequal partial volume effects distorting the results was minimized by acquiring data sets with isotropic nominal spatial resolution. All 3 DTI sequences had similar SNR. Contrast-to-noise ratio, that is, contrast between the nerve roots and the surrounding tissue, was slightly higher with rs-DTI and ss-DTI compared with sTX-DTI. This contrast is particularly important for the detection of focal or asymmetrical signal alterations (eg, FA, ADC, axial, or radial diffusivity) along nerve roots and nerves, which may indicate intraneural pathologies due to nerve compression or other neural diseases. The quantitative FA measurements did not significantly differ between the assessed DTI techniques.

Readout-segmented diffusion imaging has been shown to be a robust technique for quantitative imaging, especially in areas prone to susceptibility artifacts and consequent image distortions.[28–30] Despite the risk of motion effects corrupting data in multishot techniques, our lumbar spine images did not show according deteriorations. This robustness might be partly attributed to motion navigators used to detect and correct corrupted segments.

Apart from a slightly lower CNR, sTX-DTI, based on the dynamic parallel transmit selective-excitation technology, performed equally well as rs-DTI. The selective excitation, kept short by parallel transmission, allowed to reduce the FOV and, thus, acquisitions with sufficiently short echo times and echo trains to keep artifacts related to B0 and B1 field inhomogeneity under control, and signal intensity large enough. Nevertheless, CNR still seemed limited by the relatively long minimal echo time. This restriction, however, might be overcome with further pulse sequence developments.

As was shown in other studies,[3,4] the inclusion of a DTI evaluation of the extradural part of the nerve roots reduces the number of false-positive and false-negative findings in patients with low back pain and pain irradiation in the lower extremity. Foraminal narrowing is a common finding in elderly patients and does not necessarily imply nerve compression. On the other hand, nerve root entrapment can be related to dynamic spinal instabilities not elicited in the supine position in whole-body MR imaging.

However, long acquisition times prevented this method from being more commonly used in clinical routine. Faster acquisitions schemes may allow to gather more information on the utility of nerve root DTI in larger patient cohorts. In addition, the gain in acquisition time may be invested to increase resolution while maintaining the SNR. This is of major importance to assess the intradural nerve roots, that is, the lateral recess segment.[31] Isotropic high-resolution DTI imaging is also of importance when assessing the thicker extradural nerve components to minimize partial volume effects and to render the quantitative measurements more reliable. Our FA values are in accordance with recent DTI studies at 3 T.[3,14,15] Nonetheless, a physiological increase of FA values and a decrease of ADC along the nerve roots, as recently shown be Miyagi et al,[16] has to be considered in quantitative evaluations.

Recently, other studies compared readout-segmented and selective-excitation diffusion-weighted imaging (DWI) of prostate and breast. A study assessing the prostate found that sTX-DWI was able to provide images with comparable image quality more than 5 times faster than rs-DWI, however, at the expense of significantly increased geometric distortion.[20] In breast cancer, sTX-DWI provided significantly higher image quality, lesion conspicuity, and SNR than rs-DWI.[24] Regarding diffusion imaging of the spine, to our best knowledge, no studies comparing both acquisition techniques have been published so far.

Limitations

Certain limitations have to be acknowledged. First, the number of healthy volunteers was small, however, the data were consistent with low standard deviations. Second, no symptomatic patients were included in this study. However, to apply these techniques to a larger cohort of clinical patients, we considered it mandatory, both for ethical reasons and regarding efficiency, to first confirm robust data acquisition with the new techniques, in particular since the quantitative evaluation can be time-consuming. The small size of the lumbar nerve roots and consequent challenges with partial volume effects necessitate such robustness in combination with a careful image postprocessing to establish reliable quantitative values. In addition, the presented data may serve as basis for statistical power analysis for future larger clinical trials.

CONCLUSIONS

In summary, DTI data acquired with rs-DTI and sTX-DTI were rated higher for overall image quality and lower for severity of geometrical distortion artifacts than standard of reference ss-DTI data, despite a faster acquisition. Both techniques, rs-DTI and sTX-DTI, robustly generated images without major distortions. Thus, DTI acquisitions in the coronal plane, with fewer slices required to cover the symmetrically exiting nerve roots, may allow for functional neurography in a reasonable scan time in routine clinical practice. Apart from a slightly lower CNR in sTX-DTI, quantitative and qualitative analysis did not reveal significant differences between the 2 coronal acquisition techniques.

ACKNOWLEDGMENTS

The authors are grateful to Gustav Andreisek, MD, MBA, head of musculoskelatal and MR imaging, University Hospital Zurich, University of Zurich, Switzerland, for his valuable support.

REFERENCES

1. Aota Y, Niwa T, Yoshikawa K, et al. Magnetic resonance imaging and magnetic resonance myelography in the presurgical diagnosis of lumbar foraminal stenosis. *Spine (Phila Pa 1976)*. 2007;32:896–903.
2. Karppinen J, Malmivaara A, Tervonen O, et al. Severity of symptoms and signs in relation to magnetic resonance imaging findings among sciatic patients. *Spine (Phila Pa 1976)*. 2001;26:E149–E154.
3. Eguchi Y, Ohtori S, Orita S, et al. Quantitative evaluation and visualization of lumbar foraminal nerve root entrapment by using diffusion tensor imaging: preliminary results. *AJNR Am J Neuroradiol*. 2011;32:1824–1829.
4. Dallaudiere B, Lincot J, Hess A, et al. Clinical relevance of diffusion tensor imaging parameters in lumbar disco-radicular conflict. *Diagn Interv Imaging*. 2014;95:63–68.
5. Liang J, Wu W, Ru N, et al. Microstructural changes in compressed nerve roots are consistent with clinical symptoms and symptom duration in patients with lumbar disc herniation. *Spine (Phila Pa 1976)*. 2015. [Epub ahead of print].
6. Mori S, Zhang J. Principles of diffusion tensor imaging and its applications to basic neuroscience research. *Neuron*. 2006;51:527–539.
7. Lindberg PG, Bensmail D, Bussel B, et al. Wallerian degeneration in lateral cervical spinal cord detected with diffusion tensor imaging in four chronic stroke patients. *J Neuroimaging*. 2011;21:44–48.
8. Lindberg PG, Feydy A, Le Viet D, et al. Diffusion tensor imaging of the median nerve in recurrent carpal tunnel syndrome—initial experience. *Eur Radiol*. 2013; 23:3115–3123.
9. Chhabra A, Flammang A, Padua A Jr, et al. Magnetic resonance neurography: technical considerations. *Neuroimaging Clin N Am*. 2014;24:67–78.
10. Eppenberger P, Andreisek G, Chhabra A. Magnetic resonance neurography: diffusion tensor imaging and future directions. *Neuroimaging Clin N Am*. 2014;24: 245–256.
11. Simon NG, Lagopoulos J, Gallagher T, et al. Peripheral nerve diffusion tensor imaging is reliable and reproducible. *J Magn Reson Imaging*. 2015. [Epub ahead of print].
12. Breckwoldt MO, Stock C, Xia A, et al. Diffusion tensor imaging adds diagnostic accuracy in magnetic resonance neurography. *Invest Radiol*. 2015;50:498–504.
13. Gasparotti R, Lodoli G, Meoded A, et al. Feasibility of diffusion tensor tractography of brachial plexus injuries at 1.5 T. *Invest Radiol*. 2013;48:104–112.

14. Budzik JF, Verclytte S, Lefebvre G, et al. Assessment of reduced field of view in diffusion tensor imaging of the lumbar nerve roots at 3 T. *Eur Radiol*. 2013;23:1361–1366.
15. Chuanting L, Qingzheng W, Wenfeng X, et al. 3.0T MRI tractography of lumbar nerve roots in disc herniation. *Acta Radiol*. 2014;55:969–975.
16. Miyagi R, Sakai T, Yamabe E, et al. Consecutive assessment of FA and ADC values of normal lumbar nerve roots from the junction of the dura mater. *BMC Musculoskelet Disord*. 2015;16:156.
17. Porter DA, Heidemann RM. High resolution diffusion-weighted imaging using readout-segmented echo-planar imaging, parallel imaging and a two-dimensional navigator-based reacquisition. *Magn Reson Med*. 2009;62:468–475.
18. Holdsworth SJ, Skare S, Newbould RD, et al. Robust GRAPPA-accelerated diffusion-weighted readout-segmented (RS)-EPI. *Magn Reson Med*. 2009;62:1629–1640.
19. Azuma T, Kodama T, Yano T, et al. Optimal imaging parameters for readout-segmented EPI of the temporal bone. *Magn Reson Med Sci*. 2015;14:145–152.
20. Barth BK, Cornelius A, Nanz D, et al. Diffusion-weighted imaging of the prostate: image quality and geometric distortion of readout-segmented versus selective-excitation accelerated acquisitions. *Invest Radiol*. 2015;50:785–791.
21. Liney GP, Holloway L, Al Harthi TM, et al. Quantitative evaluation of diffusion-weighted imaging techniques for the purposes of radiotherapy planning in the prostate. *Br J Radiol*. 2015;88:20150034.
22. Thierfelder KM, Scherr MK, Notohamiprodjo M, et al. Diffusion-weighted MRI of the prostate: advantages of Zoomed EPI with parallel-transmit-accelerated 2D-selective excitation imaging. *Eur Radiol*. 2014;24:3233–3241.
23. Rosenkrantz AB, Chandarana H, Pfeuffer J, et al. Zoomed echo-planar imaging using parallel transmission: impact on image quality of diffusion-weighted imaging of the prostate at 3 T. *Abdom Imaging*. 2015;40:120–126.
24. Park JY, Shin HJ, Shin KC, et al. Comparison of readout segmented echo planar imaging (EPI) and EPI with reduced field-of-view diffusion-weighted imaging at 3T in patients with breast cancer. *J Magn Reson Imaging*. 2015;42:1679–1688.
25. Schmidt H, Gatidis S, Schwenzer NF, et al. Impact of measurement parameters on apparent diffusion coefficient quantification in diffusion-weighted-magnetic resonance imaging. *Invest Radiol*. 2015;50:46–56.
26. Landis JR, Koch GG. The measurement of observer agreement for categorical data. *Biometrics*. 1977;33:159–174.
27. Kundel HL, Polansky M. Measurement of observer agreement. *Radiology*. 2003;228:303–308.
28. Yeom KW, Holdsworth SJ, Van AT, et al. Comparison of readout-segmented echo-planar imaging (EPI) and single-shot EPI in clinical application of diffusion-weighted imaging of the pediatric brain. *AJR Am J Roentgenol*. 2013;200:W437–W443.
29. Thian YL, Xie W, Porter DA, et al. Readout-segmented echo-planar imaging for diffusion-weighted imaging in the pelvis at 3T-A feasibility study. *Acad Radiol*. 2014;21:531–537.
30. Hayes LL, Jones RA, Palasis S, et al. Drop metastases to the pediatric spine revealed with diffusion-weighted MR imaging. *Pediatr Radiol*. 2012;42:1009–1013.
31. Budzik JF, Balbi V, Verclytte S, et al. Diffusion tensor imaging in musculoskeletal disorders. *Radiographics*. 2014;34:E56–E72.